RSC Applied Polymers

ROYAL SOCIETY OF CHEMISTRY

PAPER

View Article Online
View Journal

Cite this: DOI: 10.1039/d5lp00172b

Short-side-chain composite membranes with polyaminobenzene sulfonic acid-enriched single-walled carbon nanotubes for polymer electrolyte fuel cells

Baskaran Mohan Dass,[a] Ramya Padmanaban, [a,b] Aparna Mahalingam, [a,b] Neeshma Maniprakundil,[a,b] Harshal Agarwal, [a,b] Sreekuttan M. Unni, [a,b] Vishal M. Dhavale [a,b] and Santoshkumar D. Bhat *[a,b]

This study reports the fabrication of composite membranes based on short-side-chain perfluorosulfonic acid (SSC-PFSA) polymers reinforced with polyaminobenzene sulfonic acid-functionalized single-walled carbon nanotubes (PABS-f-SWCNTs) for enhanced polymer electrolyte membrane fuel cell (PEMFC) performance. The dual-functionalized SWCNTs, enriched with $-SO_3H$ and $-NH_2$ groups, were uniformly dispersed within the SSC-PFSA matrix, promoting dipolar interactions and efficient proton conduction pathways. Comprehensive characterization confirmed improved ion exchange capacity, water uptake, thermal stability, and proton conductivity, with the 0.5 wt% PABS-f-SWCNT composite membrane exhibiting optimal performance. Under fuel cell operating conditions, this membrane demonstrated a peak power density of 1707 mW cm^{-2} at 100% RH and sustained high current density at reduced humidity, outperforming the pristine SSC-PFSA membrane. The findings highlight the synergistic role of zwitterionic functional groups and nanotube reinforcement in advancing next-generation PEMFC membrane technology.

Received 11th June 2025,
Accepted 6th August 2025

DOI: 10.1039/d5lp00172b

rsc.li/rscapplpolym

1. Introduction

Short-side-chain perfluorosulfonic acid (SSC-PFSA) membrane electrolytes have garnered attention due to their impressive ionic conductivity in polymer electrolyte membrane fuel cells (PEMFCs). SSC-PFSA membranes strike a balance between transport properties and stability, making them suitable for PEMFCs. Compared to conventional long-side-chain PFSA membranes, SSC-PFSA membranes offer better durability and enhanced proton conductivity in PEMFCs.

However, despite their higher crystallinity and water absorption properties, SSC-PFSA membranes face challenges such as diminished proton conductivity under low humidity conditions and increased hydrogen crossover through larger ionic clusters at elevated temperatures.[1,2] Addressing these issues is crucial for optimizing their performance under demanding operating conditions of PEMFCs.

Incorporating various additives into PFSA membranes is a strategy used to enhance the properties of PEMFCs.[3] These additives include inorganic fillers, functionalized nanomaterials, organic compounds, metal oxides, layered silicates and metal–organic frameworks (MOFs). Each type of additive contributes uniquely to improve the membrane's characteristics, such as proton conductivity, mechanical strength, thermal stability, and chemical resistance. Inorganic fillers like silica (SiO_2), titanium dioxide (TiO_2), and zirconium oxide (ZrO_2) are commonly used to enhance the mechanical strength and thermal stability of PFSA membranes by controlling water uptake. These fillers also create additional proton conduction pathways, especially under low humidity conditions in PEMFCs.[4–16]

Recent reports suggest that functionalized nanomaterials, such as carbon nanotubes (CNTs) and graphene oxide (GO), significantly improve the mechanical strength and thermal stability of PFSA membranes. When functionalized with groups like sulfonic acid ($-SO_3H$) or carboxylic acid (–COOH), these nanomaterials also enhance proton conductivity in composite membranes.[17]

Single-walled carbon nanotubes (SWCNTs) have gained considerable attention due to their unique structure and potential applications in various fields. Surface functionalization involves attaching organic functional groups to the surfaces of CNTs.[18] These functional groups reduce long-range van der Waals forces and enhance interactions with composite materials.[19] Functionalization of CNTs provides better dispersion in solvents and aids the dispersion of CNTs in

[a]CSIR-Central Electrochemical Research Institute-Madras Unit, CSIR Madras Complex, Chennai-600113, India. E-mail: sdbhat.cecri@csir.res.in
[b]Academy of Scientific and Innovative Research (AcSIR), Ghaziabad-201002, India

membrane electrolytes for fuel cells. SWCNTs, chemically modified with functional groups such as –COOH, can also serve as catalyst support layers in PEMFCs. Multiple functionalization routes for CNTs offer advantages for the nanocomposite membrane in terms of fuel cell performance.[20,21]

In the present study, composite membranes are formed by a unique dual functionalization approach *via* incorporating poly aminobenzene sulfonic acid (PABS)-enriched SWCNT nanoparticles into a short-side-chain perfluorosulfonic acid (SSC-PFSA) polymer and then membrane activation to enhance proton mobility and fuel cell performance at low relative humidity. Due to the highly precise structure of PABS-SWCNTs, it allows for the enrichment of $-SO_3H$ groups through functionalization.[22,23]

The PABS-SWCNTs are covalently attached to reinforce the connection with pristine SSC-PFSA. PABS-SWCNTs consist of dipolar ions formed by the presence of both $-NH_2$ and $-SO_3H$ functional groups. These dipolar ions, associated with SSC-PFSA, promote efficient ion mobility throughout the polymer and enhance the overall properties of PEMFCs.[24–26]

The physicochemical properties of the developed composite membranes, including ion exchange capacity, water uptake, swelling ratio, thermal and proton mobility, were analysed and compared with those of the pristine SSC-PFSA membrane. The fuel cell performance of the composite membrane was then explored through preparation of membrane electrode assemblies and its evaluation under typical fuel cell operating conditions.

2. Experimental section

2.1 Materials

Aquivion® (SSC-PFSA) (D-790, 25 wt%, Solvay Specialty Polymers USA, LLC), poly(*m*-aminobenzene sulfonic acid)-functionalized single-walled carbon nanotubes (PABS-f-SWCNTs) (75–85% carbon basis, $D \times L$ 1.1 nm × 0.5–1.0 μm, Sigma-Aldrich), and *N*,*N*-dimethylacetamide (DMAc) (SRL, extra pure, ≥99.5%) were employed to prepare the membranes. Sulfuric acid (H_2SO_4) was used to activate the ionic clusters of the membrane. Deionized water (resistance of 18.2 MΩ cm), obtained using a Milli-Q ultrapure water purification system and Borosil glassware, was used throughout the study.

2.2 Methods

2.2.1 Preparation of composite SSC-PFSA membranes. Composite membranes of SSC-PFSA were fabricated by incorporating the PABS-f-SWCNT copolymer as an additive into the SSC-PFSA polymer using the solution casting technique. PABS enriched with SWCNTs was added in varying weight percentages (0.25, 0.5, 0.75 and 1). Initially, a 1 wt% ionomer solution was prepared by dissolving 1 g of SSC-PFSA ionomer in 100 ml of DMAc solution. The ionomer solution was stirred continuously at room temperature for 48 h.

For membrane fabrication, 0.3 g of SSC-PFSA polymer was dissolved in an appropriate amount of DMAc at room temperature. The desired weight percentage of PABS-SWCNTs was dispersed in the polymer solution. The dispersion of Aq-PABS-f-SWCNT-0.5 is given in Fig. S1. Later, the resulting solution was subjected to constant stirring for 48 h at room temperature and then sonicated for 1 h to ensure uniform dispersion of the filler.

The resulting mixture was then cast onto a flat glass plate and dried in a vacuum oven at 80 °C for 12 h to form the polymer electrolyte membrane. For comparison, a pristine SSC-PFSA membrane was also prepared using the same process without any additive. To activate the $-SO_3H$ groups, the prepared membranes were immersed in 0.5 M H_2SO_4 for 1 h, followed by washing with deionized water. The thickness of the membranes was found to be approximately 50 ± 5 μm.

3. Results and discussion

3.1. XRD analysis

Fig. 1 shows the X-ray diffraction (XRD) patterns of pristine SSC-PFSA, PABS-f-SWCNT, and Aq-PABS-f-SWCNT composite membranes. In Fig. 1(a), the diffraction peak between 15 and 20° can be attributed to the polymer backbone networks.[27] In the PABS-f-SWCNTs, peaks were observed at 2θ values of 12.34°, 25.95°, and 43.20°, corresponding to the (001), (002), and (100) planes, respectively. These peaks are in good agreement with the JCPDS file no. 41-1487.[28]

The interlayer spacing between adjacent sp^2 graphene surfaces within SWCNTs was calculated using Bragg's law, $n\lambda = 2d \sin\theta$, where d is the spacing between graphite layers, n is the diffraction order, λ is the wavelength of X-rays, and d_{002} spacing values for hexagonal carbon in PABS-f-SWCNT, Aq-PABS-f-SWCNT-0.25, Aq-PABS-f-SWCNT-0.5, and Aq-PABS-f-

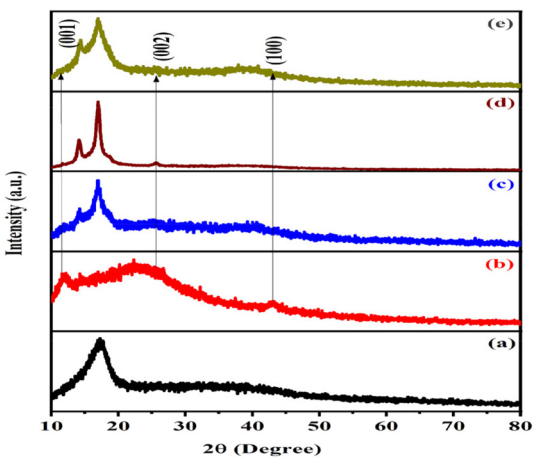

Fig. 1 XRD patterns for (a) pristine SSC-PFSA, (b) PABS-f-SWCNT, (c) Aq-PABS-f-SWCNT-0.25 wt%, (d) Aq-PABS-f-SWCNT-0.5 wt% and (e) Aq-PABS-f-SWCNT-1 wt% composite membranes.

SWCNT-1 wt% were 0.3388 nm, 0.3369 nm, 0.3364 nm, and 0.3363 nm, respectively.

The degree of graphitization for PABS-f-SWCNT, Aq-PABS-f-SWCNT-0.25, Aq-PABS-f-SWCNT-0.5, and Aq-PABS-f-SWCNT-1 wt% was found to be 89%, 60%, 82%, and 88%, respectively.

3.2. Spectral analysis

Fig. 2 presents the FT-IR spectra of pristine SSC-PFSA, PABS-f-SWCNT, and Aq-PABS-f-SWCNT composite membranes with different loadings (0.25, 0.5, and 1 wt%). The symmetric and asymmetric stretching bands observed at 1086 cm^{-1} and 1210 cm^{-1} correspond to the SO_3^- groups present in pristine SSC-PFSA. The FT-IR spectra also show peaks at 1218 cm^{-1} and 1374 cm^{-1}, which are attributed to the symmetric and asymmetric stretching vibrations of the C–F group.[29] Additionally, the stretching bands at 961 cm^{-1} and 1148 cm^{-1} correspond to the symmetric vibrations of the F–C–F and C–O–C groups, respectively. The stretching bands of the S–C and S–O groups appear at 634 cm^{-1} and 713 cm^{-1}, confirming interactions within the polymer matrix.[22]

The C–H stretching vibration is observed at 2874 cm^{-1}, while the O–H bending vibration appears at 1708 cm^{-1}.[23] The C═O stretching frequency, appearing at 1716 cm^{-1}, is characteristic of PABS-f-SWCNTs.[30] The peak at 3467 cm^{-1} is associated with the O–H functional group. In the FT-IR spectra of the Aq-PABS-f-SWCNT composite membranes, an additional peak at 3436 cm^{-1} is observed, which is not present in the pristine SSC-PFSA membrane. This shift is indicative of dipolar ion interactions between the $-NH_2$ and SO_3H ($SO_3H^+NH_2^-$) functional groups.[24]

3.3. Thermal analysis

The thermograms of the prepared polymer electrolytes are presented in Fig. 3, highlighting the thermal characteristics of pristine SSC-PFSA, PABS-f-SWCNT, and Aq-PABS-f-SWNCT composite membranes with different loadings (0.25 wt%, 0.5 wt% and 1 wt%). The results indicate that the composite membranes exhibit enhanced thermal stability compared to the pristine membrane. All the membranes display similar degradation patterns, consistent with previous studies.[31] The observed weight loss at 300 °C and 400 °C is primarily attributed to the degradation of sulfonic acid groups and the decomposition of the polymer membrane's framework respectively.

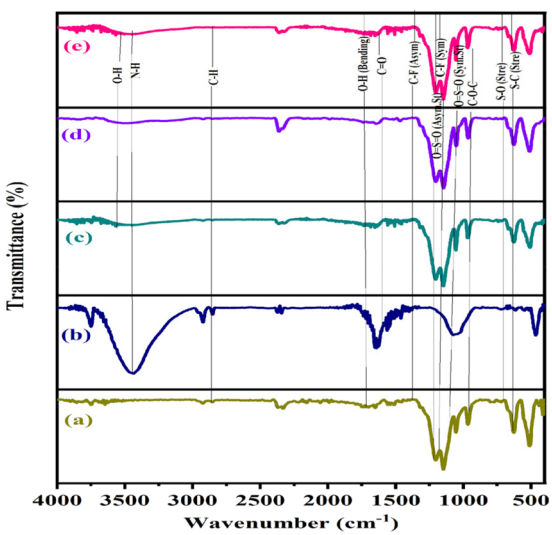

Fig. 2 FT-IR spectra for (a) pristine SSC-PFSA, (b) PABS-f-SWCNT, (c) Aq-PABS-0.25 wt%, (d) Aq-PABS-f-SWCNT-0.5 wt%, and (e) Aq-PABS-f-SWCNT-1 wt% composite membranes.

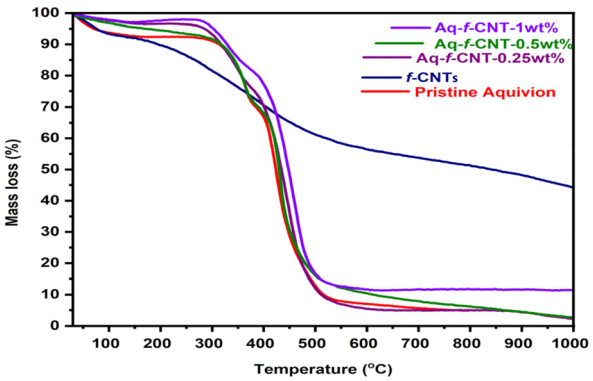

Fig. 3 Thermograms of SSC-PFSA, f-CNT and Aq-PABS-f-SWCNT composite membranes.

The thermal profile of PABS-f-SWCNTs reveals an initial weight loss. The elimination of the sulfonic acid group at around 280 °C and a significant weight loss of 14.47% at around 420 °C are due to the thermal degradation of PABS.[32] SSC-PFSA and its composite membranes showed similar thermal properties. The polymer electrolyte was thermally stable up to 250 °C. The weight loss at temperature >250 °C is due to the loss of the $-SO_3H$ group. Final polymer disintegration occurs at a temperature of around 450–500 °C.[33]

3.4. Particle size distribution and morphology

The average particle size and zeta potential of the PABS-f-SWCNT and Aq-PABS-f-SWCNT-0.5 dispersions are given in Fig. S2 and S3, respectively. Dynamic light scattering (DLS) was performed to measure the hydrodynamic diameter of the nanoparticles in solution. DLS analysis of the PABS-f-SWCNT dispersion in the SSC-PFSA ionomer reveals a *Z*-average particle size of 979 nm, indicating a highly uniform particle distribution. This dispersion is attributed to strong ionic interactions between the functionalized SWCNT surfaces and the sulfonic acid groups of the PFSA polymer, which aid in preventing aggregation and enhancing colloidal stability.

The uniform dispersion of PABS-f-SWCNTs plays a critical role in ensuring homogeneous morphology, consistent proton conduction pathways, and mechanical reinforcement throughout the membrane matrix. Zeta potential analysis was conducted to evaluate the stability of PABS-SWCNTs dispersed in an SSC-PFSA solution. The measured zeta potential was −26.2 mV. The observed zeta potential indicates that

PABS-SWCNTs are reasonably stabilized in the SSC-PFSA medium, likely due to specific interactions such as hydrogen bonding and ionic interactions. These findings support the feasibility of SSC-PFSA as a functional dispersing medium for SWCNTs in nanocomposite membrane applications.

Fig. 4 presents the atomic force microscopy (AFM) images of pristine SSC-PFSA and Aq-PABS-f-SWCNT-0.5 wt%. The AFM images of the pristine SSC-PFSA membrane exhibit a relatively smooth surface with minimal fluctuations in topography. However, the incorporation of PABS-functionalized SWCNTs alters the surface morphology due to the formation of a nanotube network within the matrix. The incorporation of f-SWCNTs increases the roughness of the membrane surface, as evidenced by the AFM topography. The root mean square (RMS) roughness of the membrane can be quantitatively analysed using AFM.

With the addition of PABS-f-SWCNTs, the surface roughness increases to 9.58 nm due to the presence of nanotubes, which introduce local protrusions. This increase in roughness can influence the hydration behaviour and water uptake of the membrane, thereby improving its performance in applications such as fuel cells or batteries, where surface interactions with water are critical.

The AFM study also provides valuable insight into the interfacial interaction between the SSC-PFSA matrix and the PABS-f-SWCNTs.[34] AFM analysis of the composite membrane reveals a uniform distribution of functionalized nanotubes, leading to more effective reinforcement in the SSC-PFSA matrix. The phase mode images presented in Fig. S4 indicate a relatively uniform dispersion of the filler within the polymer matrix. No significant phase separation is observed in the composite membrane, suggesting good compatibility between the PABS-f-SWCNTs and the SSC-PFSA matrix.

3.5. X-Ray photoelectron spectroscopy (XPS)

The XPS spectra of pristine SSC-PFSA and Aq-PABS-f-SWCNTs are shown in Fig. 5. The spectra reveal characteristic peaks corresponding to C, F, S, O and N. These peaks were analysed using a Gaussian–Lorentzian fitting approach, with background subtraction performed using the Shirley method. In pristine SSC-PFSA, fluorine exhibits a binding energy of 686.8 eV, as depicted in Fig. 5. The prominent peaks at 289.7 eV and 290.3 eV correspond to the C–F and CF_2 bonds, respectively. These binding energies are characteristic of pristine SSC-PFSA (see Fig. 5a and b). For PABS-f-SWCNTs, various carbon species were identified, with peaks for C═O, C═C (sp^2), and C–C (sp^3) observed at 287.4 eV, 282.7 eV, and 285.0 eV, respectively.[35] A broad band extending from 287.4 eV to 290.3 eV corresponds to oxygen-related molecules and a π–π^* transition. In the S 2p spectrum, the main peak at 168.2 eV is attributed to the C–SO_3 group (Fig. 5c). The positions and relative intensities of these peaks provide insight into the types of functional groups and their molecular environments in SSC-PFSA.

Fig. 5d shows the high-resolution oxygen spectra. In addition to the standard peaks at 530.2 eV and 531.2 eV, which correspond to water adsorption and the hydroxyl group (O–H) in PABS-f-SWCNTs, a satellite peak at 528.4 eV was also observed.[36] This peak is associated with oxygen species in the sample. The binding energies observed for the N 1s state (Fig. 5e) are in contrast to theoretical values and indicate good agreement between the expected and detected graphitic and amine nitrogen peaks. The broad band at around 400.1–400.7 eV was initially assigned to graphitic nitride. The typical peak for phenylamine nitrogen is usually found at around 399.3 eV, but in this study, a slightly lower binding energy 397.9 eV was observed. This difference might be due to the position of the phenyl amine nitrogen, possibly located in an adjacent vacancy or near the edge of the graphene network. High formation energy is required to create an energy gap for individual phenyl amine nitrogen atoms to expand alongside the out-

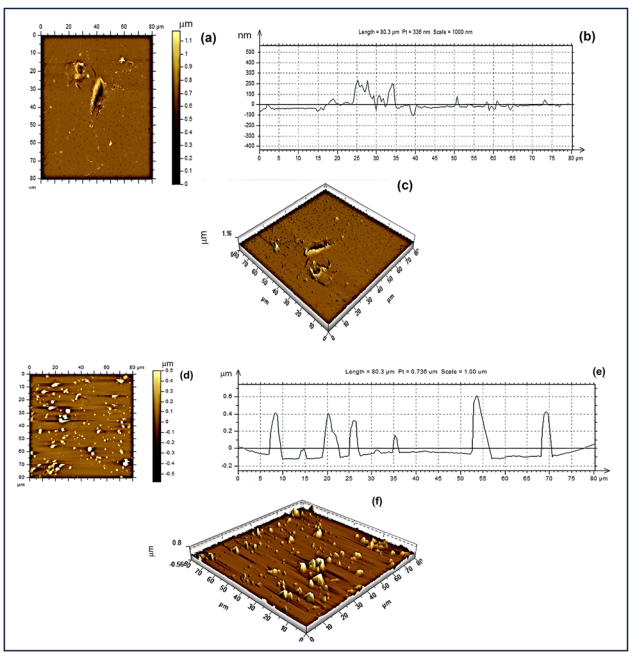

Fig. 4 AFM images of (a–c) pristine SSC-PFSA and (d–f) Aq-PABS-f-SWCNT-0.5 wt% composite membranes.

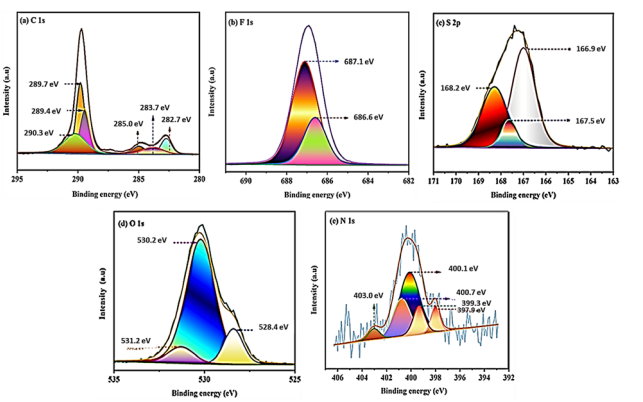

Fig. 5 (a) C 1s, (b) F 1s, (c) S 2p, (d) O 1s and (e) N 1s XPS spectra of the Aq-PABS-f-SWCNT composite membrane.

ermost graphene layer, leading to variations in their binding energies.[19] In functionalized single-walled carbon nanotubes, a significant peak at 397.9 eV was detected, which was consistent with the literature.[37]

3.6. Physico-chemical properties

3.6.1. Ion exchange capacity. In Fig. 6(a), the IEC data for the pristine SSC-PFSA membrane and composite membranes are displayed. The addition of PABS-SWCNTs can enhance the membrane's performance by increasing the number of acid-transmissible groups, which can improve ion conductivity and water absorption. The IEC of the composite material Aq-f-PABS-SWCNTs was the highest with the incorporation of 0.5 wt% f-PABS-SWCNTs. However, beyond this concentration, the IEC value decreased. This trend could be attributed to the agglomeration of f-PABS-SWCNT particles which can reduce the effective surface area available for ion exchange.[38]

3.6.2. Hydration properties and mechanical stability. Water uptake in polymer membranes is crucial for their proton conductivity and mechanical properties. The Grotthuss mechanism plays a key role in this process by facilitating the transfer of protons through a network of hydrogen-bonded water molecules, which enables efficient proton conduction. In hydrated polymer membranes, water molecules help protons hop from one site to another, creating a continuous proton-conducting network. This mechanism is particularly important for maintaining high proton conductivity in these membranes. Additionally, maintaining a balance between water uptake and mechanical stability is crucial. Excessive water absorption can lead to swelling and mechanical degradation of the polymer membrane, while insufficient water content can impede proton conduction. Achieving the right level of hydration is essential for optimizing both the performance and durability of the membrane. At higher temperatures, the water absorption behaviour of polymer membranes becomes increasingly important. To address this, several strategies can be employed such as increasing the crosslink density of the polymer to reduce water absorption, incorporating hydrophobic groups to limit water uptake, and using composite materials or blending with other substances to enhance dimensional stability. These modifications help improve the membrane's performance and durability under varying conditions. Introducing an optimal level of functionalized PABS-SWCNTs into the SSC-PFSA composite membrane enhances its water absorption capacity. This improvement is achieved by increasing the number of hydrophilic ions per unit volume, which facilitates greater water uptake compared to the pristine SSC-PFSA membrane.[39] This enhancement is visually represented in Fig. 6.

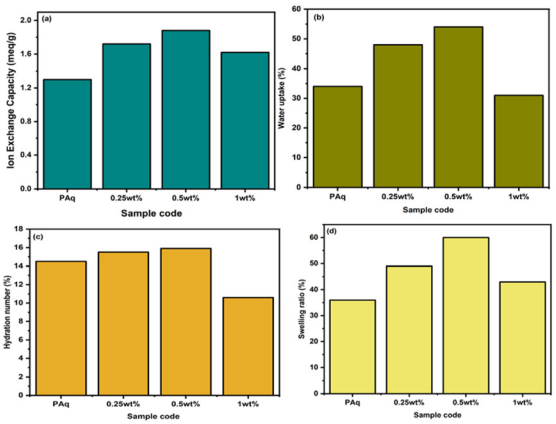

Fig. 6 Bar graphs illustrating (a) ion exchange capacity, (b) water uptake, (c) hydration number and (d) swelling ratio of both pristine SSC-PFSA and composite membranes.

The swelling behaviour and hydration number of the Aq-f-PABS-SWCNT composite membranes at various weight percentages and at ambient temperature are shown in Fig. 6(c and d). The hydration number of the Aq-f-PABS-SWCNT-0.5 wt% composite membrane was found to be the highest. This indicates improved water uptake, which can enhance the membrane's structural integrity and ion transport. In this specific Aq-f-PABS-SWCNT composite membrane, the addition of functionalized 0.5 wt% PABS-SWCNTs helps to reinforce the membrane matrix, providing better mechanical properties and stability. This enhancement is crucial for applications where the membrane is exposed to varying environmental conditions. Fig. S5 shows the stress–strain curves of the Aq-PABS-f-SWCNT-0.5 wt% composite membrane and SSC-PFSA. The Aq-PABS-f-SWCNT membrane exhibits improved mechanical stability (19.6 MPa) compared to SSC-PFSA (13.2 MPa). This improvement is attributed to the reinforcing effect of well-dispersed functionalized SWCNTs, which enhance both tensile strength and flexibility by forming strong interfacial interactions within the polymer matrix. These enhanced properties are beneficial for mechanical durability during fuel cell operation.

3.6.3. Electrochemical properties

3.6.3.1. Proton conductivity. The proton conductivity of the electrolyte membrane is a crucial factor in determining the performance of a PEMFC. Higher proton conductivity enhances ionic transfer efficiency, which directly contributes to improved power density and overall efficiency of the fuel cell. Incorporating functionalized materials, such as single-walled carbon nanotubes (SWCNTs), into polymer membranes like SSC-PFSA can significantly enhance their properties. These modifications lead to better water management, reduced membrane degradation, and ultimately higher performance in fuel cell applications. Incorporating PABS-f-SWCNTs into pristine SSC-PFSA membranes can significantly enhance proton conductivity. This is due to the unique properties of SWCNTs, such as high surface area and excellent conductivity, which can improve the overall performance of the membrane. Proton conductivity values of the prepared membranes are given in Fig. 7.

The proton conductivity of the Aq-f-PABS-SWCNT (0.5 wt%) composite membrane was higher compared to pristine SSC-PFSA. This trend demonstrates the beneficial effect of incorporating f-SWCNTs on enhancing the membrane's

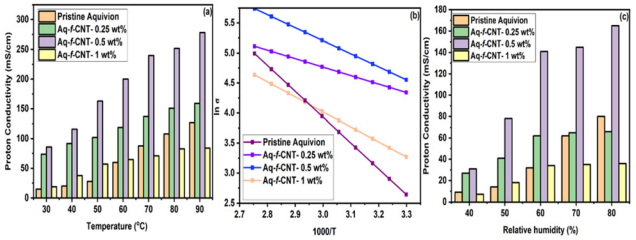

Fig. 7 (a) Proton conductivity (σ) as a function of temperature at 95% RH, (b) logarithmic plot of proton conductivity *vs.* 1000/*T*, and (c) proton conductivity at different relative humidities at 65 °C of the prepared SSC-PFSA and composite membranes.

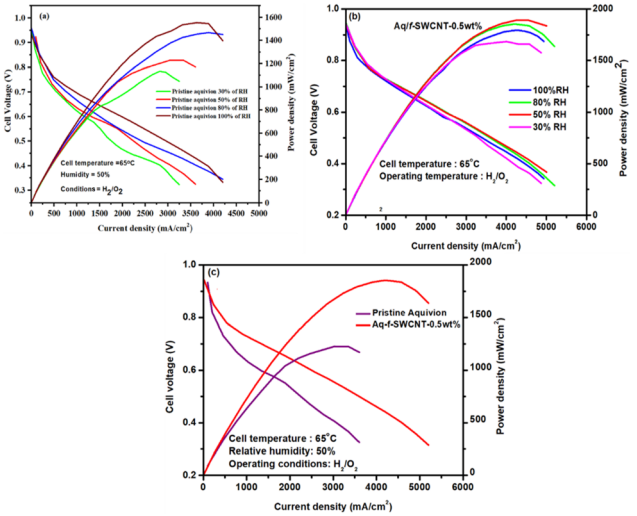

Fig. 8 (a and b) Fuel cell performance under different RH conditions at 65 °C of (a) pristine SSC-PFSA and (b) Aq-PABS-f-SWCNT-0.5 wt% membranes. (c) Comparison of the performance of SSC-PFSA and Aq-PABS-f-SWCNT-0.5 wt% membranes at 65 °C under 50% RH.

proton transport properties. The increase in proton conductivity can be attributed to the additional SO_3H, which enhances the acidic properties and water uptake of the composite membrane due to the incorporation of the f-PABS-SWCNT additive. This effect contributes to improved proton transport within the membrane, further boosting its overall performance. The inclusion of the additive not only expands the ionic nanochannels but also creates new proton-conducting sites. This happens through mechanisms like hydrogen bonding and zwitterionic interactions, significantly enhancing the proton conductivity of the membrane. The zwitterionic structure of PABS-SWCNTs plays a crucial role in enhancing proton transport. The negatively charged sulfonate groups and the positively charged amine groups create new pathways for proton conduction, allowing them to act as both proton acceptors and donors.

The dual functionality of acting as both a proton acceptor and donor, due to the zwitterionic structure of PABS-SWCNTs, significantly enhances membrane proton conductivity. This unique feature effectively boosts the membrane's efficiency, making it a powerful component in improving overall performance.[38] The proton conductivity of the Aq-f-PABS-SWCNT (1 wt%) membrane was found to be 84 mS cm^{-1}, which is low when compared to other composite membranes. This reduction of proton conductivity of the composite membrane having loading above 0.5 wt% can be attributed to agglomeration of fillers. This aggregation can hinder effective proton transport and reduce overall membrane performance. The activation energies of the composites (0.25, 0.5 and 1 wt%) were 0.027, 0.019 and 0.042 eV respectively. Upon incorporation of the functionalized nanofiller into the polymer matrix, the activation energy drastically reduced from 0.14 eV (SSC-PFSA) to 0.019 eV (Aq-PABS-f-SWCNT-0.5 wt%) which indicates the formation of a well-defined proton transport network.

3.6.3.2. Fuel cell performance and chemical stability studies. Fig. 8(a) presents the polarization data from a single cell with an active area of 5 cm^2, utilizing the PABS-f-SWCNT additive in the pristine SSC-PFSA electrolyte membrane. The study maintained Pt metal loading at 0.5 mg cm^{-2} for both the anode and the cathode. Additionally, the research explored various relative humidity (RH) conditions for both the pristine SSC-PFSA membrane and the Aq-PABS-f-SCENT-0.5 wt% composite membrane, as illustrated in Fig. 8(b). The SSC-PFSA-based MEA achieved peak power densities of 1103 and 1485 mW cm^{-2} at 30% and 100% RH, respectively. In comparison, the Aq-PABS-f-SWCNT-0.5 wt% composite membrane achieved a current density 2000 mA cm^{-2} at 0.6 V and exhibited peak power densities of 1652 and 1707 mW cm^{-2} at 30% and 100% RH, respectively. Fig. 8(c) shows that the Aq-PABS-f-SWCNT-0.5 wt% composite membrane-based MEA exhibits improved performance at lower RH, which can be attributed to the optimal concentration of PABS-functionalized SWCNTs. These SWCNTs help retain water molecules within the interfacial layer, thereby enhancing ionic conductivity and ultimately leading to increased fuel cell performance.

Fenton's test was employed to assess the oxidative stability of the membranes. The membranes were immersed in Fenton's reagent (3% H_2O_2 and 4 ppm Fe^{2+}) for 48 h at 80 °C. The initial dry weights of the samples were recorded and the weight changes were monitored at regular intervals (every 24 hours) to determine the degradation rate. After each interval, the membrane samples were thoroughly washed with deionized water and dried at 60 °C before weighing. As the concentration of the filler increases, the oxidative stability also increases, which is attributed to the radical-scavenging ability and uniform dispersion of functionalized SWCNTs within the polymer matrix. These results confirm that the inclusion of PABS-f-SWCNTs effectively enhances membrane resistance to chemical degradation. The *ex situ* durability data are given in Table S1. Fig. S6 illustrates the long-term chemical durability of the Aq-PABS-f-SWCNT-0.5 wt% composite membrane compared to a benchmark SSC-PFSA membrane, evaluated under open circuit voltage (OCV) conditions for 50 hours at low RH (30%). This test simulates harsh fuel cell operating environments where the membrane is exposed to chemical attack

from crossover gases (H_2 and Air) without the benefit of humidification or current flow, making it a rigorous method to assess membrane stability and resistance to radical-induced degradation.

Over the 50-hour test, the Aq-PABS-f-SWCNT-0.5 wt% membrane maintains a higher and more stable cell voltage compared to the SSC-PFSA membrane. The initial OCV of the Aq-PABS-f-SWCNT membrane is approximately 0.95 V and it gradually decreases to 0.87 V, maintaining about 90% of the initial OCV. In contrast, the SSC-PFSA membrane begins at a slightly lower OCV (~0.91 V) and degrades more rapidly, falling to ~0.8 V, maintaining about 87% of OCV over the same duration.

The OCV retention of the Aq-PABS-f-SWCNT membrane can be attributed to the incorporation of 0.5 wt% functionalized SWCNTs, which likely serve as radical scavengers and reinforce the polymer matrix, thereby inhibiting chemical degradation. In addition, the cross-over current density for the prepared composite membrane after the 50 hours chemical stability test was measured and is represented in Fig. S7. Fig. S7 presents the hydrogen crossover behaviour of the Aq-PABS-f-SWCNT-0.5 wt% composite membrane, measured using linear sweep voltammetry (LSV) in a H_2/N_2 configuration. Hydrogen gas was supplied to the anode and nitrogen gas was supplied to the cathode. Any hydrogen permeating through the membrane is oxidized at the cathode, producing a current directly proportional to the rate of hydrogen crossover.

At low voltages, a sharp increase in current density is observed due to the rapid oxidation of crossover hydrogen. The current transitions from a negative to positive value, reaching a plateau in the range of 0.15–0.25 V. This reflects the membrane's capability to restrict hydrogen diffusion effectively. The low and stable current density (8.2 mA cm^{-2}) suggests limited hydrogen permeability, attributed to the presence of well-dispersed functionalized single-walled carbon nanotubes (f-SWCNTs), which restricts the fuel cross-over.

These results demonstrate the improved *in situ* chemical durability of the Aq-PABS-f-SWCNT composite membrane under low humidity operating conditions, highlighting its potential for durable performance in next-generation PEM fuel cells where low humidity tolerance is crucial.

4. Conclusions

This study presents the development of an Aq-PABS-f-SWCNT composite membrane using a short-side-chain-based PFSA. Notably, the proton conductivity of the Aq-PABS-f-SWCNT-0.5 wt% composite membrane surpasses that of the pristine SSC-PFSA membrane at 95% RH, measuring 278 mS cm^{-1}. Cell performance tests on a single fuel cell further highlight the superior efficacy of the Aq-PABS-f-SWCNT-0.5 wt% composite membrane compared to the pristine SSC-PFSA membrane. The SSC-PFSA-based MEA achieved peak power densities of 1103 and 1485 mW cm^{-2} at 30% and 100% RH, respectively. In comparison, the Aq-PABS-f-SWCNT-0.5 wt% composite membrane achieved a current density of 2000 mA cm^{-2} at 0.6 V and exhibited peak power densities of 1652 and 1707 mW cm^{-2} at 30% and 100% RH, respectively.

Author contributions

Baskaran Mohan Dass: conceptualization, data curation, formal analysis, and methodology; Ramya Padmanaban: writing – review & editing; Aparna Mahalingam: writing – review & editing; Neeshma Maniprakundil: writing – review & editing; Harshal Agarwal: funding acquisition; Sreekuttan M. Unni: funding acquisition; Vishal M. Dhavale: funding acquisition; Santoshkumar D. Bhat: methodology, project administration, resources, and supervision.

Conflicts of interest

There are no conflicts to declare.

Data availability

The data supporting this article have been included as part of the SI.

Supplementary information is available. Materials Characterization, Preparation of membrane electrode assembly, Physico-chemical studies, particle size and zeta potential, Mechanical properties, AFM Phase mode images, Chemical Stability, Oxidative stability and Hydrogen crossover studies. See DOI: **https://doi.org/10.1039/d5lp00172b**.

Acknowledgements

The authors thank the CSIR-Fast track translational (FTT060503) project for the financial assistance.

References

1 Y. Garsany, R. W. Atkinson, M. B. Sassin, R. M. E. Hjelm, B. D. Gould and K. E. S. Lyson, Improving PEMFC performance using short-side-chain-low-equivalent-weight PFSA ionomer in the cathode catalyst layer, *J. Electrochem. Soc.*, 2018, **165**(5), F381–F391.

2 S. Siracusano, V. Baglio, A. Stassi, L. Merlo, E. Moukheiber and A. S. Arico, Performance analysis of short-side-chain SSC-PFSA perfluorosulfonic acid polymer for proton exchange membrane water electrolysis, *J. Membr. Sci.*, 2014, **466**, 1–7.

3 C. Y. Wong, W. Y. Wong, K. Ramya, M. Khalid, K. S. Loh, W. R. W. Daud, K. L. Lim, R. Walvekar and A. A. H. Kadhum, Additives in proton exchange membranes for low and high-temperature fuel cell applications, *Int. J. Hydrogen Energy*, 2019, **44**, 31463–31484.

4 S. Hwang, H. G. Lee, Y. G. Jeong, C. Choi, I. Hwang, S. H. Song, S. Y. Nam, J. H. Lee and K. Kim, Polymer electrolyte membranes containing functionalized organic/inorganic composite for polymer electrolyte membrane fuel cell applications, *Int. J. Mol. Sci.*, 2022, **23**(22), 14252.
5 K. T. Adjemian, R. Dominey, L. Krishnan, H. Ota, P. Majsztrik, T. Zhang, J. Mann, B. Kirby, G. Gatto, M. V. Simpson, J. Leahy, S. Srinivasan, J. B. Benziger and A. B. Bocarsly, Function and characterization of metal oxide-Nafion composite membranes for elevated-temperature H_2/O_2 PEM fuel cells, *Chem. Mater.*, 2006, **18**(9), 2238–2248.
6 S. Paul, S. J. Choi and H. J. Kim, Enhanced proton conductivity of a Zn(II)-based MOF/SSC-PFSA composite membrane for PEMFC applications, *Energy Fuels*, 2020, **34**(8), 0067–10077.
7 V. S. Velan, G. Velayutham, N. Hebalkar and K. S. Dhathathreyan, Effect of SiO_2 additives on the PEM fuel cell electrode performance, *Int. J. Hydrogen Energy*, 2011, **36**(22), 14815–14822.
8 K. T. Adjemian, S. Srinivasan, J. Benziger and A. B. Bocarsly, Investigation of PEMFC operation above 100 °C employing perfluorosulfonic acid silicon oxide composite membranes, *J. Power Sources*, 2002, **109**(2), 356–364.
9 X. Wu and K. Scott, A PFSA composite membrane with sulfonic acid functionalized TiO_2 nanotubes for polymer electrolyte fuel cells and water electrolysers, *Fuel Cells*, 2013, **13**(6), 1138–1145.
10 G. Mohammadi, M. Jahanshahi and A. Rahimpour, Fabrication and evaluation of Nafion nanocomposite membrane based on ZrO_2–TiO_2 binary nanoparticles as fuel cell MEA, *Int. J. Hydrogen Energy*, 2013, **38**(22), 9387–9394.
11 T. Nakajima, T. Tamaki, H. Ohashi and T. Yamaguchi, Introduction of size-controlled Nafion/ZrO_2 nanocomposite electrolyte into primary pores for high Pt utilization in PEFCs, *J. Electrochem. Soc.*, 2012, **160**(2), F129.
12 E. M. Alosime, A review on surface functionalization of carbon nanotubes: methods and applications, *Discover Nano*, 2023, **18**(1), 12.
13 G. Rambabu, D. S. Bhat and M. L. Figueiredo, Carbon nanocomposite membrane electrolytes for direct methanol fuel cells - A concise review, *Nanomaterials*, 2019, **9**(9), 1292.
14 N. Jha, P. Ramesh, E. Bekyarova, X. Tian, F. Wang, M. E. Itkis and R. C. Haddon, Functionalized single-walled carbon nanotube-based fuel cell benchmarked against US DOE 2017 technical targets, *Sci. Rep.*, 2013, **3**, 2257.
15 J. Liu, Y. Yuan and S. Bashir, Functionalization of aligned carbon nanotubes to enhance the performance of fuel cell, *Energies*, 2013, **6**(12), 6476–6486.
16 G. Sivasubramanian, K. Hariharasubramanian, P. Deivanayagam and J. Ramaswamy, High-performance SPEEK/SWCNT/fly ash polymer electrolyte nanocomposite membranes for fuel cell applications, *Polym. J.*, 2017, **49**(10), 703–709.
17 A. Shukla, P. Dhanasekaran, S. Sasikala, N. Nagaraju, S. D. Bhat and V. K. Pillai, Nanocomposite membrane electrolyte of polyaminobenzene sulfonic acid grafted single walled carbon nanotubes with sulfonated polyether ether ketone for direct methanol fuel cell, *Int. J. Hydrogen Energy*, 2019, **44**(50), 27564–27574.
18 P. Guan, Y. Zou, M. Zhang, W. Zhong, J. Xu, J. Lei and Y. Zhang, High-temperature low-humidity proton exchange membrane with "stream-reservoir" ionic channels for high-power-density fuel cells, *Sci. Adv.*, 2023, **9**(17), 1386.
19 M. Ferrari, J. Catalano, M. G. Baschetti, A. M. G. De and G. C. Sarti, FTIR-ATR study of water distribution in a short-side-chain PFSI membrane, *Macromolecules*, 2012, **28**, 1901–1912.
20 J. Li, M. Pan and H. Tang, Understanding short-side-chain perfluorinated sulfonic acid and its application for high temperature polymer electrolyte membrane fuel cells, *RSC Adv.*, 2014, **4**, 3944–3965.
21 M. K. Hansen, D. Aili, E. Christensen, C. Pan, S. Eriksen, J. O. Jensen, J. H. Von Barner, Q. Li and N. J. Bjerrum, PEM steam electrolysis at 130 °C using a phosphoric acid doped short side chain PFSA membrane, *Int. J. Hydrogen Energy*, 2012, **37**, 10992–11000.
22 N. Zhao, D. Edwards, C. Lei, K. Wang, J. Li, Y. Zhang, S. Holdcroft and Z. Shi, The importance of water transport on short-side chain perfluorosulfonic acid membrane fuel cells operating under low relative humidity, *J. Power Sources*, 2013, **242**, 877–883.
23 S. Subianto, S. Cavaliere, D. J. Jones and J. Roziere, On electrospinning of PFSA: A comparison between long and short-side chain ionomers, *ECS Trans.*, 2011, **41**, 1517–1520.
24 M. Neeshma, P. Dhanasekaran, S. M. Unni and S. D. Bhat, Short side perfluorosulfonic acid composite membrane with covalently grafted cup stacked carbon nanofibers for polymer electrolyte fuel cells, *J. Membr. Sci.*, 2023, **668**, 121240.
25 R. D. Amato, A. Donnadio, C. Battocchio, P. Sassi, M. Pica, A. Carbone, I. Gatto and M. Casciola, Polydopamine coated CeO_2 as radical scavenger filler for SSC-PFSA membranes with high proton conductivity, *Materials*, 2021, **14**, 528.
26 S. Paul, S. J. Choi and H. J. Kim, Enhanced proton conductivity of a Zn(II)-based MOF/SSC-PFSA composite membrane for PEMFC applications, *Energy Fuels*, 2020, **34**(8), 10067–10077.
27 M. Huda, T. Kawahara, J. H. Park, M. Kawasumi and Y. Matsuo, Single-walled carbon nanotubes supported Pt electrocatalyst as a cathode catalyst of a single fuel cell with high durability against start-up/shut-down potential cycling, *ACS Appl. Energy Mater.*, 2023, **6**(24), 12226–12236.
28 Z. Wang, D. Ba, F. Liu, P. Cao, T. Yang, Y. Gu and H. Gao, Synthesis and characterization of large area well-aligned carbon nanotubes by ECR-CVD without substrate bias, *Vacuum*, 2005, **77**(2), 139–144.
29 D. Hou, K. Li, R. Ma and Q. Liu, Influence of order degree of coaly graphite on its structure change during preparation of graphene oxide, *J. Materiomics*, 2020, **6**(3), 628–641.

30 T. I. T. Okpalugo, P. Papakonstantinou, H. Murphy, J. McLaughlin and N. M. D. Brown, High resolution XPS characterization of chemical functionalised MWCNTs and SWCNTs, *Carbon*, 2005, **43**(1), 153–161.
31 E. M. Jackson, P. E. Laibinis, W. E. Collins, A. Ueda, C. D. Wingard and B. Penn, Development and thermal properties of carbon nanotube-polymer composites, *Composites, Part B*, 2016, **89**, 362–373.
32 B. Zhao, H. Hu, A. Yu, D. Perea and R. C. Haddon, Synthesis and characterization of water soluble single-walled carbon nanotube graft copolymers, *J. Am. Chem. Soc.*, 2005, **127**(22), 8197–8203.
33 A. Selim, I. Ayyubov, E. Talas, I. Borbath and A. Tompos, Functionalized carbon nanostructures for PEMFCs, in *Handbook of Functionalized Carbon Nanostructures*, ed. A. Barhoum and K. Deshmukh, Springer, Cham, 2024.
34 K. D. Kreuer, On the development of proton conducting polymer membranes for hydrogen and methanol fuel cells, *J. Membr. Sci.*, 2001, **185**, 29–39.
35 M. T. Martínez, M. A. Callejas, A. M. Benito, M. Cochet, T. Seeger, A. Anson, J. Schreiber, C. Gordon, C. Marhic, O. Chauvet, J. L. G. Fierro and W. K. Maser, Sensitivity of single wall carbon nanotubes to oxidative processing: structural modification, intercalation and functionalisation, *Carbon*, 2003, **41**(12), 2247–2256.
36 A. Goldoni, R. Larciprete, L. Gregoratti, B. Kaulich, M. Kiskinova, Y. Zhang, H. Dai, L. Sangaletti and F. Parmigiani, X-ray photoelectron microscopy of the C 1s core level of free-standing single-wall carbon nanotube bundles, *Appl. Phys. Lett.*, 2002, **80**(12), 2165–2167.
37 S. Trabia, K. Choi, Z. Olsen, T. Hwang, J. D. Nam and K. J. Kim, Understanding the thermal properties of precursor-ionomers to optimize fabrication processes for ionic polymer-metal composites (IPMCs), *Materials*, 2018, **11**(5), 665.
38 J. Wang, C. Gong, S. Wen, H. Liu, C. Qin, C. Xiong and L. Dong, A facile approach of fabricating proton exchange membranes by incorporating polydopamine functionalized carbon nanotubes into chitosan, *Int. J. Hydrogen Energy*, 2019, **44**, 6909–6918.
39 G. Wang, J. Kang, S. Yang, M. Lu and H. Wei, Influence of structure construction on water uptake, swelling and oxidation stability of proton exchange membranes, *Int. J. Hydrogen Energy*, 2024, **50**, 279–311.